Article

Spatio-Temporal Evaluation of GPM-IMERGV6.0 Final Run Precipitation Product in Capturing Extreme Precipitation Events across Iran

Aydin Bakhtar [1], Akbar Rahmati [2], Afshin Shayeghi [3], Javad Teymoori [4], Navid Ghajarnia [5,*] and Peyman Saemian [6]

1   Department of Water Engineering, Urmia University, Urmia 5756151818, Iran; aydinbakhtar@gmail.com
2   Department of Irrigation and Drainage Engineering, College of Abureyhan, University of Tehran, Tehran 6718773654, Iran; akbarrahmatiziveh@gmail.com
3   Water Engineering Department, Imam Khomeini International University (IKIU), Qazvin 3414916818, Iran; afshin.shayeghi@gmail.com
4   School of Civil Engineering, University of Tehran, Tehran 6718773654, Iran; javad.teymoori.419@gmail.com
5   Department of Physical Geography, Bolin Centre for Climate Research, Stockholm University, SE-10691 Stockholm, Sweden
6   Institute of Geodesy (GIS), University of Stuttgart, Geschwister-Scholl-Street 24, 70174 Stuttgart, Germany; peyman.saemian@gis.uni-stuttgart.de
*   Correspondence: navid.ghajarnia@natgeo.su.se

Abstract: Extreme precipitation events such as floods and droughts have occurred with higher frequency over the recent decades as a result of the climate change and anthropogenic activities. To understand and mitigate such events, it is crucial to investigate their spatio-temporal variations globally or regionally. Global precipitation products provide an alternative way to the in situ observations over such a region. In this study, we have evaluated the performance of the latest version of the Global Precipitation Measurement-Integrated Multi-satellitE Retrievals (GPM-IMERGV6.0 Final Run (GPM-IMERGF)). To this end, we have employed ten most common extreme precipitation indices, including maximum indices (Rx1day, Rx5day, CDD, and CWD), percentile indices (R95pTOT and R99pTOT), and absolute threshold indices (R10mm, R20mm, SDII, and PRCPTOT). Overall, the spatial distribution results for error metrics showed that the highest and lowest accuracy for GPM-IMERGF were reported for the absolute threshold indices and percentile indices, respectively. Considering the spatial distribution of the results, the highest accuracy of GPM-IMERGF in capturing extreme precipitations was observed over the western highlands, while the worst results were obtained along the Caspian Sea regions. Our analysis can significantly contribute to various hydrometrological applications for the study region, including identifying drought and flood-prone areas and water resources planning.

Keywords: climate change; extreme precipitation indices; global precipitation products; GPM-IMERG

1. Introduction

Extreme precipitation events have a significant effect on many facets of the water systems e.g., [1–5]. Such events result in floods and droughts that cause manifold problems with various socio-economical to political aspects [6–8]. Monitoring and forecasting such events play a vital role in mitigating their adverse event and is the key for resilience water resource management [9].

Precipitation extremes have happened at a higher frequency and with more intensity over the recent decades [10]. Such a dramatic shift in the precipitation patterns has already been observed in various regions including Iran, a country with an arid to a semi-arid climate located in the Middle East [11]. Between December 1998 and January 2002, Iran among many other Middle East countries faced a prolonged meteorological drought period

resulting in significant socio-economic and environmental impacts. Furthermore, within 2008–2009, Iran observed an unprecedent drought which triggered several water related issues including the acceleration of the groundwater withdrawal over the majority of its plains [12–16]. More recently, in January 2019, heavy rainfalls resulted in country-wide flood events that caused more than 78 deaths and about 1136 injuries [17]. Moreover, about 36 percent of the country's road network was damaged and 725 bridges were completely washed away [18]. Based on the governmental estimation, the above-mentioned events cost a record of more than 2.2 billion USD [19]. In contrast to the flood events in 2019, Iran has observed its driest year within the last four decades over the preceding year [20].

Over the recent decades, several high-resolution precipitation products have been developed due to development of the remote sensing techniques and the enhancement of the computational capacities [21–23]. Different precipitation satellite based precipitation products were examined using various statistical metrics over the whole Iran or some parts of the countries [24–30]. The satellite-based precipitation products with their high spatio-temporal resolution have enriched our knowledge on the statistics of the precipitation extremes [31]. Meanwhile, Hardware and software differences, in addition to following various approaches, could facilitate the records by capturing extremes and anomalies [32,33]. GPM is an international mission that provides a deep understanding of precipitation on the Earth. The GPM observatory core was launched in February 2014 in collaboration with NASA and the Japan Space Agency. This mission improves the quality and quantity of precipitation measuring as it provides records with high spatio-temporal consistency, leading to a better understanding of precipitation variability on Earth [34]. GPM-IMERG Version 6 is the latest version of GPM, which has a higher spatio-temporal resolution than its successor (TRMM). The high spatiotemporal resolution of GPM-IMERG (30 min and $0.1° \times 0.1°$) and its combination with broad coverage from north to south of the IMERG is highly regarded for extreme events studies [35–37].

Different studies were carried out to assess the performance of GPM-IMERG products in different spatial extents including global, regional, and local scales [38–49]. Among the abovementioned studies [37,39,41,42] found that GPM-IMERGF was outperformed other products and GPM-IMERG late and early versions in terms of different statistical metrics across China. Furthermore, in two studies across Netherland and Canada GPM-IMERGF were evaluated against in situ data and marked as a reliable source of precipitation for this region at daily and hourly time steps [39,43]. Evaluating the accuracy of GPM-era in multiple complex terrain regions for global scale were also showed that GPM-IMERGF and GPM-IMERGF and GSMaP Version 7 were superior upon other products in different regions [38].

Previous studies have examined extreme precipitation events over the entire Iran or its basins [50–58]. The above-mentioned studies have observed a strong positive trend in the extreme precipitation events across Iran, particularly over the northern coastal areas and western highlands of Zagros Mountains. Refs. [59,60] have shown that satellite-based products vastly underestimated extreme precipitation events, mostly in wet regions while being able to capture such events over southwestern parts of Iran. Some recent studies have evaluated GPM-IMERGF over Iran and its basins [61–66]. However, to the best of our knowledge, the literature lacks a comprehensive assessment of the GPM-IMERGF product in detecting the extreme events over Iran. This study offers a comprehensive assessment of the GPM-IMERGF dataset in estimating extreme events over Iran. We have analyzed the performance of GPM-IMERGF against a network of consistent in situ observations at daily time scale from 2007 to 2016. To this end, we have included the latest version (V06) of the GPM-IMERGF together with the gauged precipitation at the 281 synoptic stations within 2007–2016.

We acknowledge the necessity of having a reliable near-real time precipitation estimation dataset for flood prediction and warning systems. However, there are also other applications of precipitation products in which extreme precipitation play key role as well. For example, when studying historical flood records to construct floodgates with gabion

fortifications, having a reliable record of extreme precipitation values is needed over the study area. Or when investigating extreme hazards and natural disasters, having access to precipitation datasets with accurate estimations of historical extreme values are also important. Considering the fact that GPM-IMERGF is a grid summary of precipitation, and in our study area there are large areas with no rain gauge stations and interpolating might results in poor understanding of extreme precipitation events, therefore evaluation of GPM-IMERGF in terms of correctly simulating the extreme precipitation is relevant and necessary. In addition, GPM-IMERG final version is the gauge adjusted version of GPM-IMERG and in most previous studies it has performed far better than other versions in capturing spatio-temporal variability of precipitation in various regions [47,48]. On the other hand, most studies of extreme precipitation events in Iran are related to the frequency of such events and changes in their pattern over time. Therefore, it seems that due to the lack of unreliable in situ data in Iran, bias-adjusted precipitation products are receiving more attention from various stockholders rather than near-real time products.

Our finding improves characterization of the spatio-temporal consistent view of extreme precipitation events. Iran enjoys diversity of climate regions including arid and semi-arid to fully humid region. Therefore, the findings of this study show the performance of the GPM-IMERGF V6 over various climate regions which can be utilized by the stockholders, researchers, and policymaker over regions with heterogenous climates. Considering the rise in the frequency of flood and drought events, such evaluations are necessary for various hydro-metrological applications and water resources management planning.

2. Materials and Methods

2.1. Study Area

Iran, as one of the Middle East countries, is located within the latitudes of 25–39° N and the longitudes of 40–64° E. The country is surrounded by the Alborz Mountain range in the north and Zagros Mountain ranges in the western and southwestern parts (Figure 1). These two mountain chains make the country among the most complex terrain across the Middle East, with its average elevation increasing drastically from −28 to 5610 m above sea level across Iran. However, the central parts are mostly covered by deserts. Owing to dominant complex topography, the spatio-temporal pattern of precipitation is highly variable across Iran. Mean annual precipitation in Iran is approximately 250 mm/year, with decreasing trend over recent years [67]. The spatial variation of precipitation range from <50 mm/year on extra arid low-elevation regions (Kavir and Lut deserts) to >1600 mm/year in northern areas close to the Caspian Sea [61]. According to the recent climatic classifications based on Demartone aridity index [68], Iran's climates can be categorized to Arid (A), Extra-Arid (EA), Semi-Arid (SA), Mediterranean (M), and Semi-Humid (SH) climates, while the southern shores of the Caspian Sea enjoy Humid (H) and Per-Humid (PH1 and PH2) climates [69,70]. Figure 1 illustrates climate regions and spatial distribution of IR-IMO (Islamic Republic of Iran Meteorological Organization) stations and the study area's topographical map.

2.2. Datasets

2.2.1. Reference Dataset

The evaluation of the GPM-IMERGV6.0 Final Run (GPM-IMERGF hereafter) has been conducted against a set of high-quality synoptic stations provided by the Islamic Republic of Iran Meteorological Organization (IRIMO). IRIMO is responsible for recording hourly and daily precipitation and the quality control is carried out by IRIMO and could be considered as the most reliable data across the country [52,71].

Daily data from a total of 281 stations across Iran within ten years from 2007 to 2016 has been collected in this study for the analyses (Figure 1).
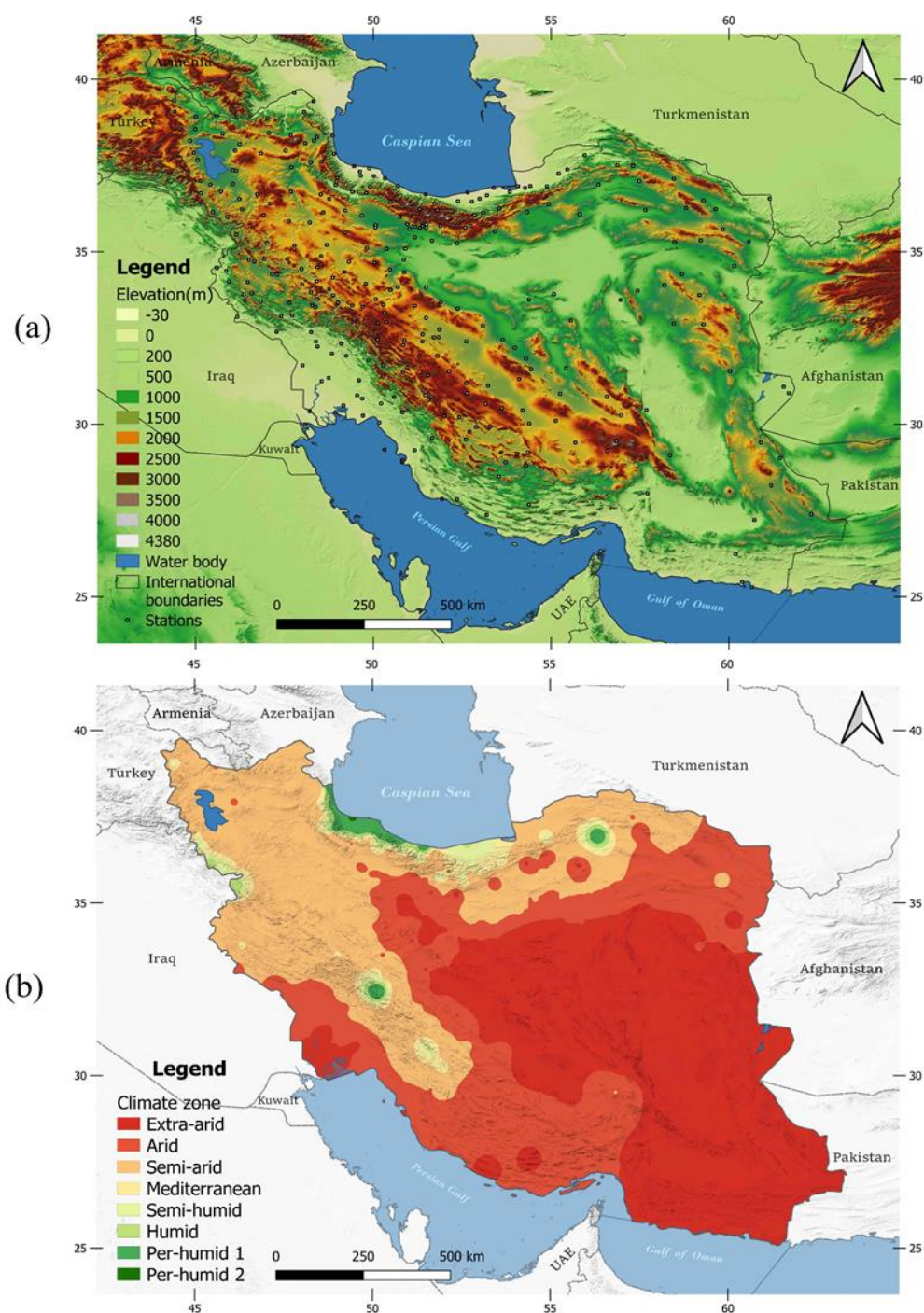
Figure 1. Topographical (**a**) and climate map (**b**) of the Iran [69,70] IRIMO stations are shown in black squares along with the topographical map.

The reference dataset does not properly spatially cover the whole area of the study area. We argue that the spatial coverage would not affect our analysis due two main reasons. First, synoptic stations are the most accurate observational rain gauges in Iran, and in our study, we have included all available synoptic stations across Iran to evaluate the performance of the GPM-IMERGF dataset. Second, many of the poorly gauged regions in the central and eastern of Iran are mainly deserts or dried areas with annual precipitation of around zero mm/year. Therefore, despite the lack of gauged precipitation over some regions, our analysis would serve as a fair and comprehensive assessment of the GPM-IMERGF dataset in estimating extreme events.

In order to consider this limitation in the study, the evaluations have been conducted based on different climatic zones. To this end, we categorized the whole study area based on different climate zones, of which, every climate enjoys maximum available synoptic stations. In this way, we have aggregated error indices in different climate zones with an adequate number of observational stations that can satisfy statistical conclusions.

2.2.2. GPM-IMERGF

The idea behind IMERG applicants is a combination of passive microwaves and infrared data from a large ensemble of satellite imagery and radar satellites [72]. GPM-IMERG combines precipitation measurements from 9 international satellites: GPM, GCOM-W1, NOAA-18, NOAA-19, DMSP F-16, DMSP F-17, DMSP F-18, Metop-A, and Metop-B [73]. Dual-frequency precipitation radar (DPR) and GPM microwave imager (GMI) are two distinctive features of the GPM core observatory. Although GPM utilizes only two measuring instruments compared to the five in TRMM, combining these two instruments is more valuable for achieving scientific purposes. Evaluating algorithms, detecting solid precipitation or sensitivity to light rainfall, and the cloud process are among the GPM instrument's key capabilities [74]. DPR with two bands (Ku and Ka bands) measures the three-dimensional structure of precipitation, which can measure the intensity of precipitation, snow, rain, and ice. The GMI tool, with four channels more than TRMM, allows GPM to measure rainfall intensity and types in different layers of the clouds [75]. The GMI instrument offers well-calibrated, multi-band, wide-swath observation throughout 13 channels [76]. The spatial coverage of GPM is between latitude from 65 degrees north to 65 degrees south that stretches approximately to the Arctic and Antarctic Circles, however, TRMM covers only tropical and subtropical regions [77]. In this study, the recently released (June 2021) version (V06) of IMERG mission Final Run with a spatial resolution of 0.1° and temporal resolution of 1-day is evaluated over Iran within 2007–2016. The IMERG algorithm combines, calibrates, and interpolates precipitation estimations from various sources, including microwave estimates, microwave-calibrated infrared estimates, and in situ observations [78]. The IMERGV6.0 data are available globally with three different versions Early run (with the latency of 4 h after observation time), Late run (with the latency of 14 h after observation time), and Final run (with the latency of 3.5 months after the observation time) to meet different user requirements for different purposes [79]. To provide reliable precipitation estimations for research purposes, the GPM-IMERGF uses the Global Precipitation Climatology Center (GPCC) monthly precipitation along with the European Centre for Medium-Range Weather Forecasts (ECMWF) data for calibration [78]. The GPM-IMERGF derived from the half-hourly GPM_3IMERGHH. The derived result represents the daily accumulated precipitation estimation.

The four different precipitation fields of the IMERG data are classified as calibrated precipitation (precipitationCal), uncalibrated precipitation (precipitationUncal), infrared (IR) geostationary satellite precipitation data (IRprecipitation), and precipitation extracted from merging high-quality passive microwave (PMW) sensors (HQprecipitation). PrecipitationCal which represents records after the final post-processing is considered the most reliable IMERG precipitation estimate [78]. The latter is used in the current study for the evaluations.

2.3. Extreme Precipitation Indices

To evaluate the performance of GPM-IMERGF in capturing extreme precipitation events, we have employed ten extreme precipitation indices defined by the Expert Team on Climate Change Detection and Indices (ETCCDI) (see Table 1).

Table 1. List of extreme precipitation indices used in this study.

Category	Index	Description	Definition	Unit
Maximum indices	Rx1day	Maximum 1-day precipitation	Maximum 1-day precipitation	mm
	Rx5day	Maximum 5 days of consecutive precipitation	Maximum 5 days of consecutive precipitation	mm
	CDD	Consecutive Dry Days	Annual largest number of consecutive days with daily precipitation < 1 mm	days
	CWD	Consecutive Wet Days	Annual largest number of consecutive days with daily precipitation $\geq$ 1 mm	days
Percentile indices	R95pTOT	Very wet days	The 95th percentile of daily precipitation on days $\geq$ 1 mm	mm/days
	R99pTOT	Extremely wet days	The 99th percentile of daily precipitation on days $\geq$ 1 mm	mm/days
Absolute threshold indices	R10mm	Count of heavy precipitation days	Annual number of days when precipitation $\geq$ 10 mm	days
	R20mm	Count of very heavy precipitation days	Annual number of days when precipitation $\geq$ 20 mm	days
	SDII	Simple precipitation intensity index	The ratio of precipitation on wet days to number of wet days	mm/day
	PRCPTOT	Wet-day precipitation	total amount of precipitation on days with $\geq$1 mm precipitation	mm

These indices are of great importance within the context of climate change and rising global warming [80]. Among the abovementioned indices, Rx1day and Rx5day can be utilized as a useful indices for flash floods and landslides as they are representing magnitude of extreme precipitation events. Similarly, the frequency of heavy and very heavy precipitation events is characterized by R10mm and R20mm. However, drought conditions are characterized by CDD (dry) and CWD, R95Ptot, and R99pTOT (wet) indices, respectively. Therefore, they can be very helpful for agricultural activities as they are indirectly representing dry and wet period [81]. Furthermore, all other indices could be very helpful when combined with each other.

To better examine the performance of GPM-IMERGF we divided extreme precipitation indices into three separate groups: maximum indices, percentile indices, and absolute indices [82,83].

2.4. Evaluation Approach

Global precipitation estimation models provide their outputs in a spatially aggregated format and grid cells, while most observational and reference datasets are point sources and not spatially representative of the area. Therefore, there have been two main approaches in the literature for facing this spatial inconsistency in the model and observational data. In the first approach, as suggested by the reviewer, the reference dataset is firstly aggregated in space with a chosen interpolation method that can be as simple as IDW or more advanced and complicated geospatial methods. Then the comparison is made, and error indexes are calculated accordingly. In the second approach that is followed in this study, the error indexes are firstly calculated by direct comparison of gridded data with point source observations and then, in the end, aggregated in space to present the area-averaged error values. Both of these methods have their own advantages and disadvantages; however, the critical point is that uncertainties of spatial aggregation will ultimately impact the final results in both methods but in different stages of the calculation (in the first method

when making the spatially aggregated reference dataset and in the second method when aggregating the error indexes in space). In a comprehensive evaluation of 44 gridded precipitation studies in Iran, both aforementioned methods compared the results with each other [62]. The outcome of that study proved that the ranking of the datasets would remain similar in both pointwise (second approach as defined above) and pixel-wise (first approach as defined above) approaches [62].

In this study, we have deliberately followed the point-to-pixel approach to evaluate the GPM-IMERGF over Iran as the interpolation of the synoptic stations to grids would add error to the assessment. To evaluate the performance of GPM-IMERGF in capturing precipitation extremes, we have conducted the following steps. Initially, the De Martonne aridity index [68] was calculated for all synoptic stations for the period 2007–2016. This index is one of the most commonly used aridity indices with good accuracy in identifying dry/humid conditions of different regions (see Appendix A for more information).

The evaluation is divided in different climate zones to verify if the performance of IMERGF differs in different climate conditions or not. This can have important implications for model development and enhancement, as well as providing a better and more in-depth evaluation across the study area and scientific contribution to the literature. In addition, As the stations for the whole country are unevenly distributed and most stations were scattered along western and northern parts of the country, a minority of stations were scattered across central and eastern parts of the country. As such, we categorized the whole study area based on different climate zones, of which, every climate enjoys some stations. In this way, regions that suffer from low station density can be associated with the result from the same climate zones and the results can be generalized to other regions with the same climate.

Later, the annual means of ETCCDI indices were calculated at each station. Finally, trend analysis was used to evaluate the performance of GPM-IMERGF in capturing the trend of all extreme precipitation indices for the study region.

2.4.1. Performance Metrics

The accuracy of GPM-IMERGF precipitation product was assessed using the Kling-Gupta efficiency (KGE) index along with its three main components; correlation coefficient I, bias (β), and variability component (γ). The KGE score varies between $-\infty$ to 1 (Equation (1)), with a perfect score of 1 [84,85]. In the following equations, r measures the Pearson correlation coefficient (CC) (Equation (2)), β measures the bias component defined as the ratio between average observed and estimated values with a perfect score of 1 (Equation (3)), and γ with a perfect score of 1 stand for the variability ratio as defined by the ratio of the estimated and observed coefficients of variations (Equation (4)). μ_O and μ_E indicate the average values for the observational data and estimated times series, respectively, while σ_O and σ_E stand for the standard deviations of observations and estimations. n is the number of records in the time series with valid observed or estimated data (number of records excluding the no-data values in the time series). O_i and E_i also stand for the reference and estimated data.

$$\text{KGE} = 1 - \sqrt{(r-1)^2 + (\beta-1)^2 + (\gamma-1)^2} \tag{1}$$

$$r = \frac{1}{n} \sum_1^n \frac{(O_i - \mu_O) * (E_i - \mu_E)}{\sigma_O * \sigma_E} \tag{2}$$

$$\beta = \frac{\mu_E}{\mu_O} \tag{3}$$

$$\gamma = \frac{\frac{\sigma_E}{\mu_E}}{\frac{\sigma_O}{\mu_O}} \tag{4}$$

2.4.2. Trend Analysis

Trend analysis provides valuable information regarding climate change impacts across the study region. In this study, the trends in GPM-IMERGF based precipitation indices were compared with indices based on gauge observations. The Kendall nonparametric test [86,87] was used to identify the annual trends in extreme precipitation indices.

3. Results and Discussion

3.1. Maximum Precipitation Indices

Figure 2 shows the spatial distribution of KGE, CC, bias, and VR indices for different maximum precipitation indices across the study area. The KGE scores ranged from around −8.87 for CWD to approximately 0.95 for Rx5day across various regions, indicating the varying performance of the GPM-IMERGF in matching maximum extreme precipitation indices. Considering the KGE score, it is worth mentioning that 65%, 42%, 47%, and 64% of the stations for Rx1day, Rx5day, CDD, and CWD lay below 0.3, showing that GPM-IMERGF has low accuracy in most stations of the country. The spatial pattern of KGE for all maximum indices showed that many stations scattered along with the northern parts of the country, particularly the northern coastal areas, stand for the worst results. However, GPM-IMERGF showed reasonable accuracy (KGE > 0.5) across some western regions in the Zagros mountainous areas.

Analyzing the results of Rx1day showed that climate regions including Arid, Extra-Arid, and Humid had a relatively better KGE score than other climate regions; furthermore, in these regions, GPM-IMERGF had a correlation coefficient ranging between 0.3 to 0.5, and bias and VR values were close to the optimal value. However, the worst results were observed in Semi-Humid and Per-Humid1 climates, mainly scattered along with the coastal areas of the Caspian Sea. Bias and VR indicated that GPM-IMERGF had underestimation (<0.8) broadly. For the other climates, acceptable results were not observed based on the KGE score.

Considering the Rx5day index, climate regions including Arid, Semi-Arid, and Humid had a relatively high KGE. The correlation coefficient lies between 0.6 to 0.7, which significantly impacts the KGE score. Furthermore, the variability ratio and bias were close to the optimal value (except for Humid climate, which has a relatively low bias compared to the other two regions). Similar to the Rx1day index, the worst performance of GPM-IMERGF was observed in Per-Humid1 climate that has a significant low variability ratio (VR < 0.77) estimate of less than 0.62 and largely underestimate (bias < 0.65) Rx5day for this region.

The results for the CDD index showed that GPM-IMERGF had a relatively higher KGE in Arid, Semi-Arid, and Extra-Arid climates compared to others with a correlation coefficient of about 0.5, the VR and the bias values the optimal range for these three regions. However, the worst performance of this GPM-IMERGF was observed in the Per-Humid2 climate. Although, VR and bias were approximately close to the optimal value in terms of their median value, the very low correlation coefficient significantly affects the KGE score in this climate region.

Considering the CWD index, the results showed that the GPM-IMERGF performance was superior in the Humid class, with a relatively significant difference compared to other climate regions. The correlation coefficient of 0.64 and the optimal bias and VR values have led to the excellent performance of GPM-IMERGF in this region. Similar to Rx1day and Rx5day index, the worst performance of GPM-IMERGF was observed in Per-Humid1 climate with a negative KGE score (−0.2); the low KGE score in this region was mainly because of negative CC value. Considering the climatic regions of Iran and its complex topography, the results for the KGE and its components showed relatively higher accuracy across Zagros chains, and poor performance of GPM-IMERGF was also found in humid northern areas. Overall, the spatial distribution of all metrics and wetness classes indicated that arid regions, dominant across Iran, receive higher accuracy than wet regions, particularly across northern coastal areas and central Alborz.
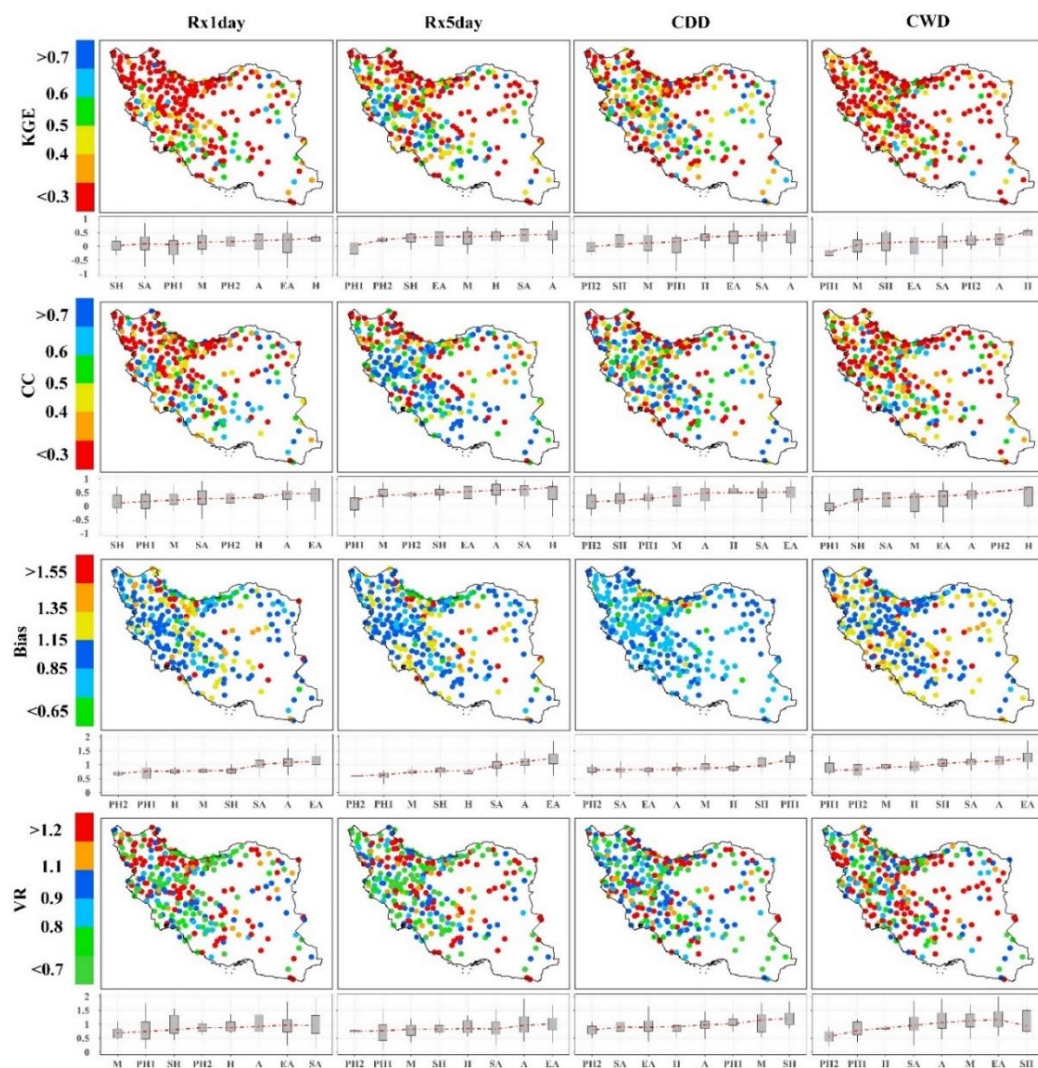
Figure 2. Reliability of GPM-IMERGV6.0 Final Run (GPM-IMERGF) in capturing maximum precipitation indices based on bias, correlation coefficient (CC), variability ratio, and Kling-Gupta efficiency (KGE) error metrics.

Figure 3 illustrates the temporal change of maximum precipitation indices over different climate regions throughout the study period (2007–2016). The results revealed that GPM-IMERGF shows lower performance in capturing the trend of maximum precipitation indices across various wet climates rather than arid to semi-arid regions. The results also show that GPM-IMERGF generally underestimates Rx1day and Rx5day over regions with the Mediterranean to PH2 climate while the underestimation increased by the wetness of the region which is consistent with [88].
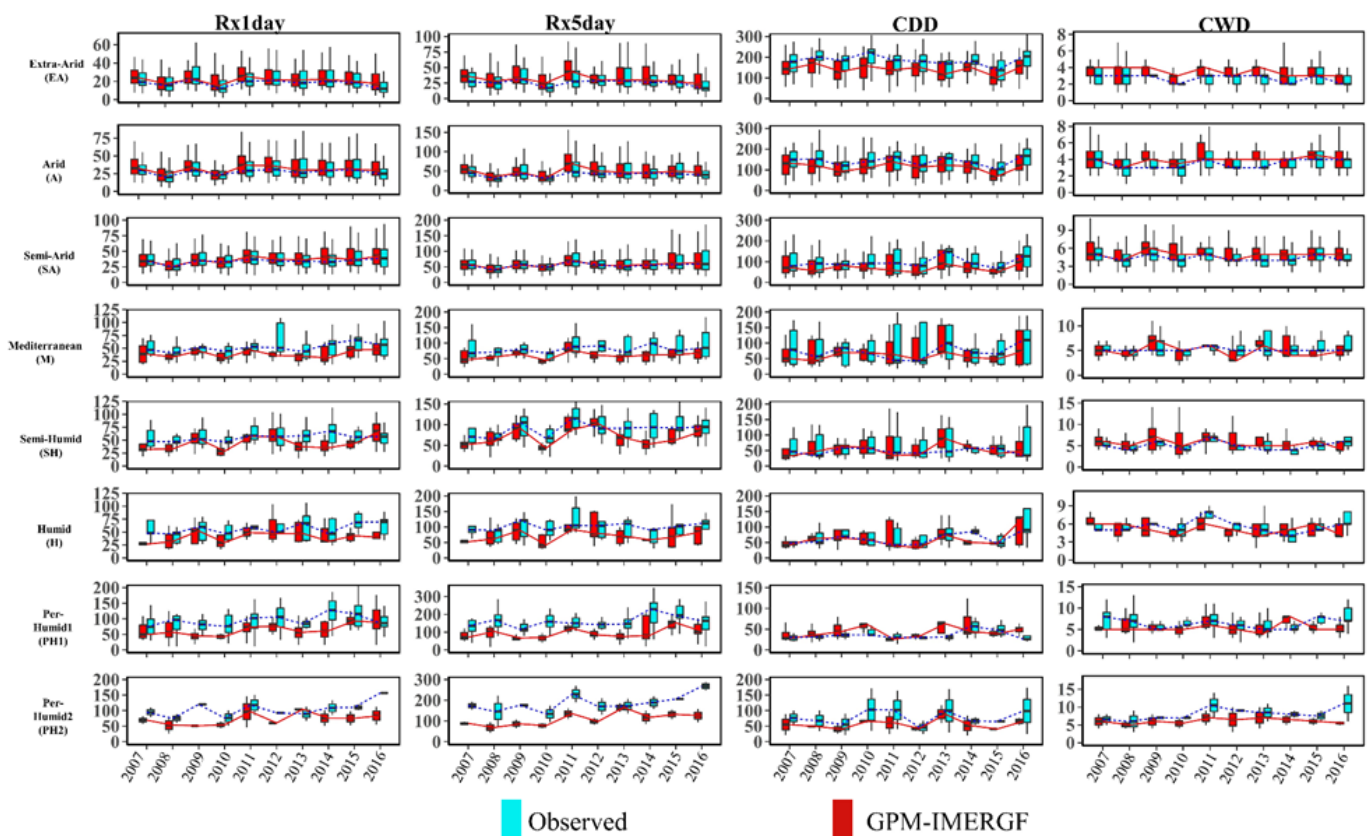
Figure 3. Temporal behavior of GPM-IMERGF in capturing maximum precipitation indices beside corresponding indices based on synoptic stations throughout 2007 to 2016.

The performance of the datasets improves in terms of CDD and CWD from Per-Humid2 to Extra-Arid climates. A slight overestimation is observed for arid and Semi-Humid regions regarding CWD index with no particular pattern for other wetness classes. It is worth mentioning that significant overestimation by GPM-IMERGF for wet regions might be due to its calibration procedure and its auxiliary sources. GPM-IMERGF utilizes ERA5 estimations for bias correction through its calibration procedure [78]. Previous results from various studies [30,88,89] suggested that ERA5 largely overestimates precipitation across humid regions, so the consequence of a high bias rate for ERA5 might reflect on GPM-IMERGF estimations.

3.2. Percentile Precipitation Indices

Figure 4 shows the spatial distribution of KGE, CC, bias, and VR metrics for percentile indices. Overall, the performance of GPM-IMERGF based on KGE in percentile indices does not follow a specific pattern in different regions of the study area with relatively good performance along Zagros mountains. The percentage of stations with KGE < 0.3 for R95pTOT and R99pTOT were 58% and 75%, respectively. However, the unfavorable results of GPM-IMERGF in the Caspian Sea strip are primarily due to the more considerable underestimation of bias and VR components of KGE, such that in terms of these two indices, Per-Humid1, Per-Humid2, and Mediterranean climates had low values. GPM-IMERGF performance for KGE has been somewhat better in R95pTOT than R99pTOT, which is estimated to be due to the high CC value in the study area, especially in some Zagros mountains. Moreover, the KGE range in different climates for GPM-IMERGF was between 0.11 to 0.28 for R95pTOT index, and R99pTOT was between −0.34 to 0.25. Furthermore, in both indices, the best KGE score for the GPM-IMERGF was observed in Humid climate, mainly due to the optimal value of bias and VR components of KGE.
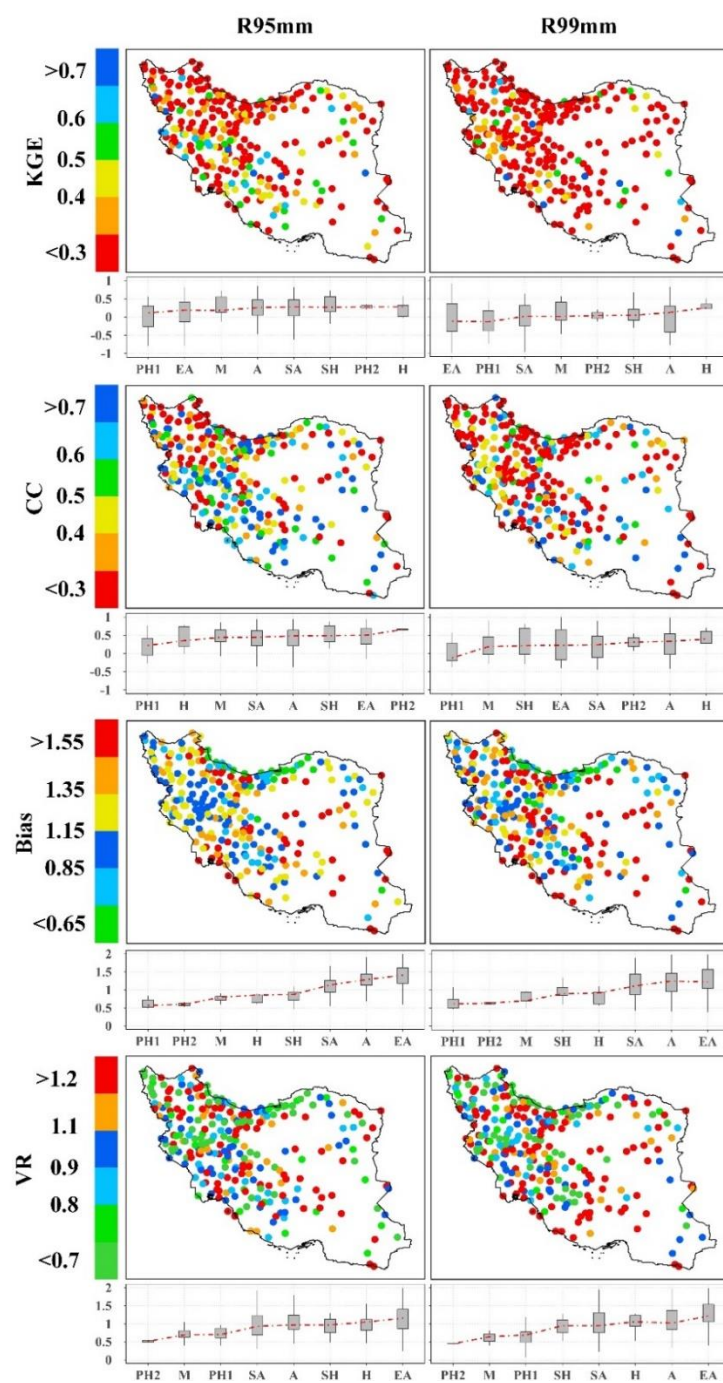
Figure 4. Reliability of GPM-IMERGV6.0 Final Run (GPM-IMERGF) in capturing percentile precipitation indices based on bias, correlation coefficient (CC), variability ratio, and Kling-Gupta efficiency (KGE) error metrics.

Figure 5 illustrated the temporal change of percentile indices for different climate regions throughout the study period from 2007 to 2016. Analyzing the trend of R95pTOT indices had shown that GPM-IMERGF had good accordance with observations in capturing the overall trend of R95pTOT. However, GPM-IMERGF slightly overestimated R95pTOT at arid classes while largely underestimated R95pTOT for the humid classes. Compared to other regions, GPM-IMERGF significantly underestimated R95pTOT for the Per-Humid1 and Per-Humid2 regions.
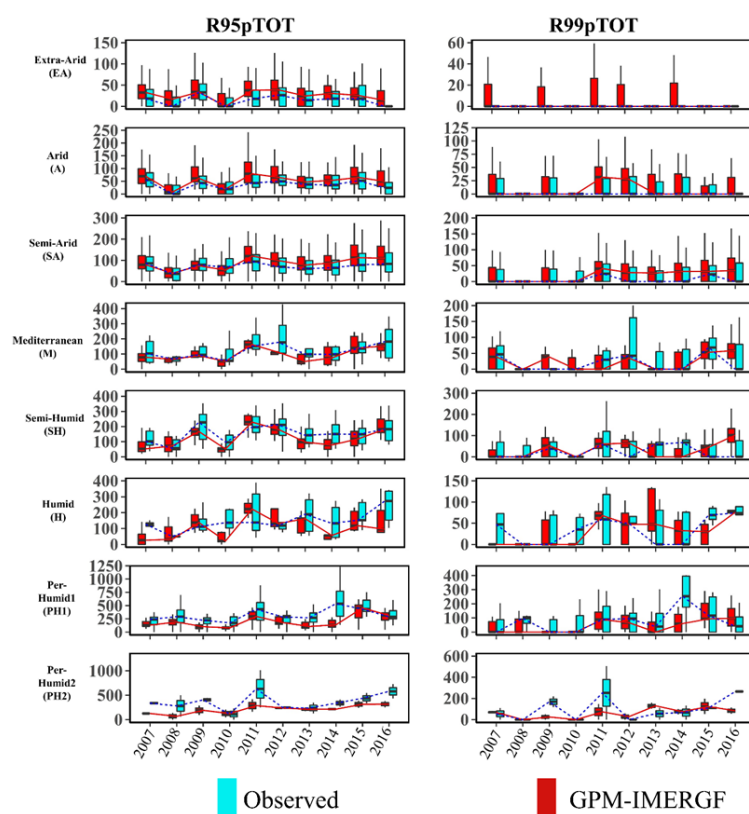
Figure 5. Temporal behavior of GPM-IMERGV6.0 Final Run (GPM-IMERGF) in capturing maximum precipitation indices beside corresponding indices based on synoptic stations throughout 2007 to 2016.

On the contrary, the overall performance of GPM-IMERGF in capturing the temporal trend of R99pTOT across all wetness classes was not acceptable. The results of GPM-IMERGF for R99pTOT were not acceptable and failed to capture the quantity and trend of R99pTOT throughout the study period. Overall, the results showed that GPM-IMERGF showed reletivaly reliable performance considering R95pTOT compared to R99pTOT index. Our finding for R95pTOT and R99pTOT is partially consistent with previous results obtained from [83] and [60]. They suggested that satellite-based precipitation products largely underestimated highly rainy days precipitation indices (e.g., R95pTOT and R99pTOT) across whole Iran and southwestern parts of Iran, respectively.

3.3. Absolute Threshold Precipitation Indices

Figure 6 shows the spatial distribution of bias, CC, VR, and KGE measures for absolute indices. The results showed that low KGE scores (<0.3) were found for approximately 43%, 63%, and 42% of stations for R10mm, R20mm, and SDII, respectively, by GPM-IMERGF across various regions. Moreover, the results revealed that low KGE scores were mainly distributed across Alborz and northern Zagros mountains. However, GPM-IMERGF had relatively reasonable accuracy (0.4–0.6) across the central Zagros mountains. Furthermore, the results showed that GPM-IMERGF was following observational data in capturing the PRCPTOT index. The best results for GPM-IMERGF in capturing PRCPTOT were obtained across the Zagros mountains and eastern Alborz regions. Overall, the KGE score results and other metrics showed that GPM-IMERGF had low to high accuracy in capturing absolute threshold indices. Moreover, there were some encouraging results for the central Zagros, which defines some areas of interest for implementing GPM-IMERGF estimations for detecting extreme precipitation events in this region.
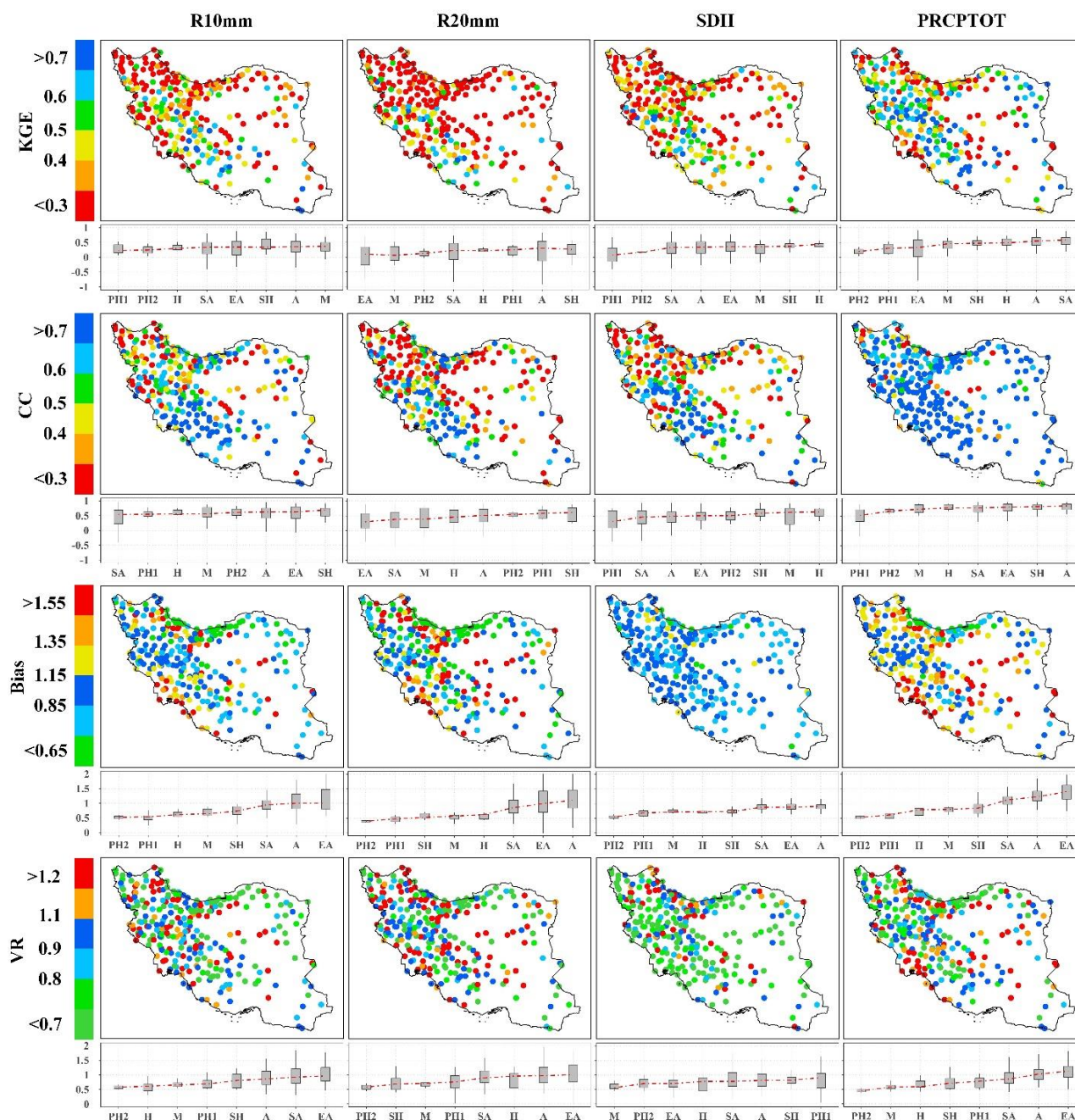
Figure 6. Reliability of GPM-IMERGV6.0 Final Run (GPM-IMERGF) in capturing absolute threshold precipitation indices based on bias, correlation coefficient (CC), variability ratio, and Kling-Gupta efficiency (KGE) error metrics.

In the matter of absolute threshold indices, the results showed that GPM-IMERGF was in good accordance with three Humid, Mediterranean, and Semi-Humid regions compared to others. However, the worst performance was observed in Per-Humid1 and Per-Humid2 climates for approximately all absolute threshold indices (except for R20mm).

Regarding R10mm, it can be acknowledged that the best results of GPM-IMERGF were observed along the Zagros Mountains. Furthermore, all climatic regions except Per-Humid1 and Per-Humid2 range between 0.3 to 0.4 in terms of median KGE. Moreover, GPM-IMERGF receives lower KGE values in wet climates regarding the R10mm index. Lower KGE values are mainly due to the significant under-estimation in the bias (bias < 0.65) and the combined effect of the low variability ratio (VR < 0.7). However, GPM-IMERGF

is in good accordance with in situ data; the CC term ranged from 0.54 to 0.69 in all climate regions. Compared to R10mm, GPM-IMERGF had a lower KGE score, such that KGE < 0.3 was scattered along 42% and 63% of stations for R10mm and R20mm, respectively. Moreover, stations located in the Zagros Mountains have performed better than other areas in terms of KGE. The performance of GPM-IMERGF in different climates in terms of KGE (in wet and dry climates) does not have the same pattern, such that the worst performance was observed in Mediterranean climate (KGE < 0.07) and the best performance was observed in climates Semi-Humid, Arid, Per-Humid1, with KGE varying around 0.25.

The main reason behind the poor performance of GPM-IMERGF for KGE values in R20mm is related to low CC value, such that the percentage of stations with CC < 0.3 has increased from 20% in the R10mm to 37% in R20mm. It is important to note that the range of bias and VR changes has not changed significantly in different climates compared to R10.

Analyzing the performance of GPM-IMERGF for SDII showed that better KGE results mainly were scattered along the Zagros mountains. Furthermore, the results for the Humid and Semi-Humid climates were superior to other regions. The results also showed that Per-Humid1 and Per-Humid2 stand for the worst performance based on GPM-IMERGF results. Spatial distribution of bias index for SDII showed that 50% of the stations have lied between optimal value for GPM-IMERGF. Meanwhile, 53% of stations had a low variability ratio (VR < 0.8). These indicate that high CC values have mainly influenced the high KGE for some regions regarding SDII in the study area.

The KGE results of PRCPTOT for the GPM-IMERGF showed that the KGE score has significantly improved in most stations in the study area (above 0.6, 35% of stations) and (below 0.3, 25% of stations) GPM-IMERGF was superior to other extreme indices in terms of KGE performance. Regarding PRCPTOT, it is worth mentioning that the high performance of GPM-IMERGF was also found in some parts of the northeastern area, as well as the Zagros mountains. It should be noted that the KGE values of GPM-IMERGF in the Caspian Sea strips have been affected by the noticeable low bias and VR index, such that even high CC values have not increased the value of KGE. Considering climate regions, GPM-IMERGF receives the lowest KGE value (KGE < 0.3) Per-Humid1 and Per-Humid2, however, it was well-performed in Semi-Arid and Arid classes with KGE of 0.59 and 0.56, respectively.

Figure 7 shows the temporal variation of absolute threshold indices calculated by the GPM-IMERGF product and its corresponding gauge values. Overall, analyzing temporal variations of GPM-IMERGF indices with gauge-based indices showed that GPM-IMERGF had acceptable accuracy in capturing the overall behavior of the gauge-based indices. The results showed that GPM-IMERGF showed a consistent pattern for all indices, such that it slightly underestimated or matched with gauge-based indies throughout 2007 to 2017 for the arid regions. Whereas, for the humid regions, GPM-IMERGF significantly underestimated all absolute indices for all years.

Overall, based on various error metrics, the results showed that GPM-IMERGF estimations were relatively reliable for absolute threshold indices compared to other indices. The higher accuracy for SDII and PRCPTOT might result from their inherent formulation procedure as they consider the total precipitation amount in their calculation steps. Our findings for southwestern parts of Iran for SDII index were totally against [60], who reported that TRMM satellite showed lower accuracy considering SDII. However, our results for PRCPTOT index were consistent. One significant difference between TRMM and GPM-IMERGF for this particular area might be due to GPM-IMERGF improvement through its complicated calibration with ERA5 and GPCC information [78].
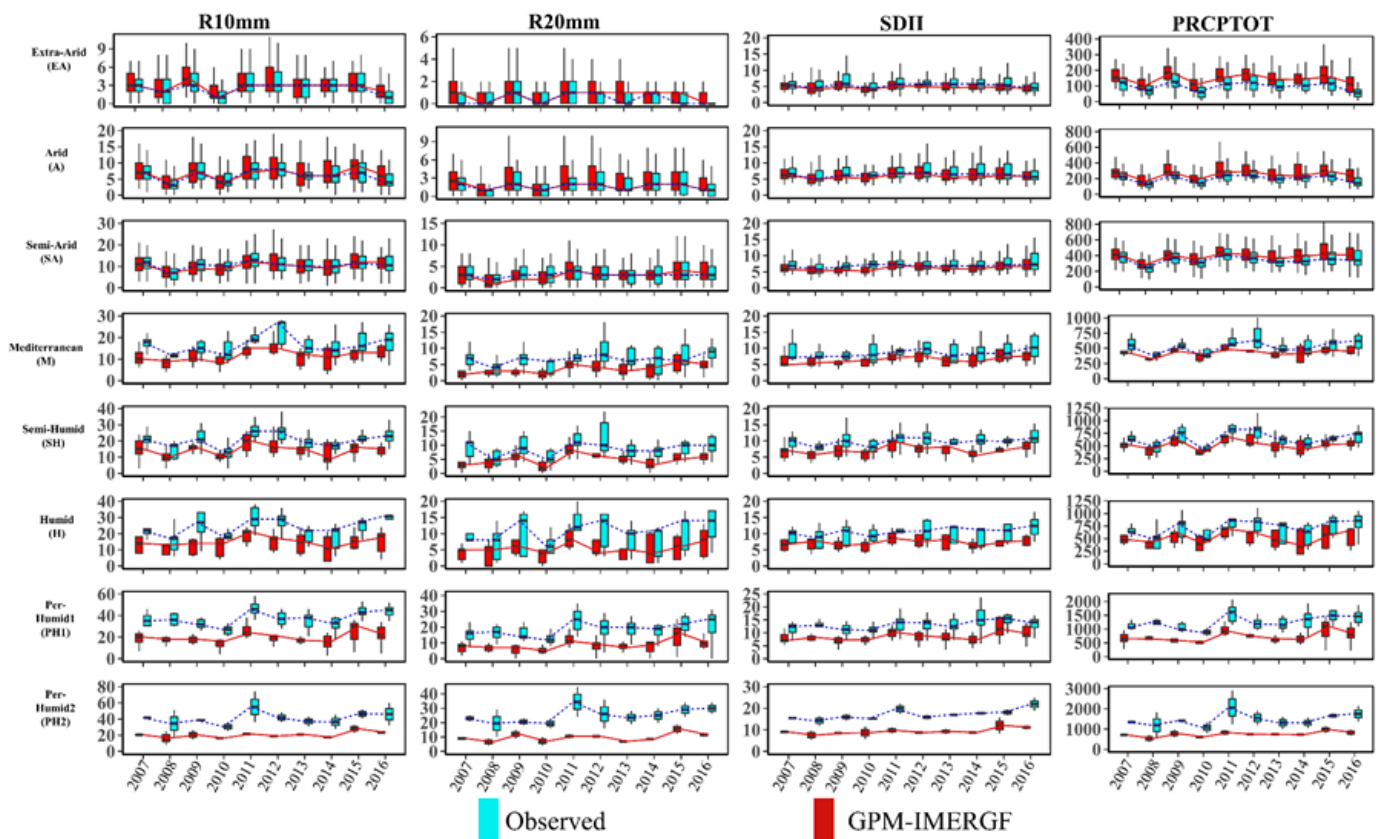
Figure 7. Temporal behavior of GPM-IMERGF in capturing maximum precipitation indices beside corresponding indices based on synoptic stations throughout 2007 to 2016.

3.4. Trend Analysis

To determine the performance of GPM-IMERGF in estimating the trend of precipitation extremes, we have compared the trend in the indices from in situ measurement and the GPM-IMERGF dataset within the study period (2007–2016). To obtain the trends, we have employed the Mann–Kendall test.

Figure 8 shows an overall agreement between the observed and estimated patterns. Regarding Rx1day and Rx5day, it is evident that GPM-IMERGF is in good accordance with in situ observation (AE < 0.3) in most regions. Considering CDD, it is worth mentioning that negative trends over the south of the Zagros Mountains with PH1 and SA climate regions have been well captured by the GPM-IMERGF (AE < 0.3). The trend analysis for the CWD index showed that the observed positive trend over the southwest, the coastal areas in the north, and the highlands of Zagros is well captured by GPM-IMERGF (AE < 0.3).

Additionally, for other regions, GPM-IMERGF captured the negative trend of CWD with acceptable accuracy (AE < 0.3). Overall, both datasets show a positive trend over the coast of Caspian and the western part of the Zagros Mountains. At the same time, it depicts a clear negative trend over the high latitudes of Zagros and arid and extra arid regions. Considering Rx1day, Rx5day, CDD, and CWD, it is evident that areas with negative trends were scattered across dry regions (Extra-Arid, Semi-Arid, and Arid), while positive trends were mainly found across humid areas regions (Humid, Semi-Humid, Per-Humid1, and Per-Humid2).
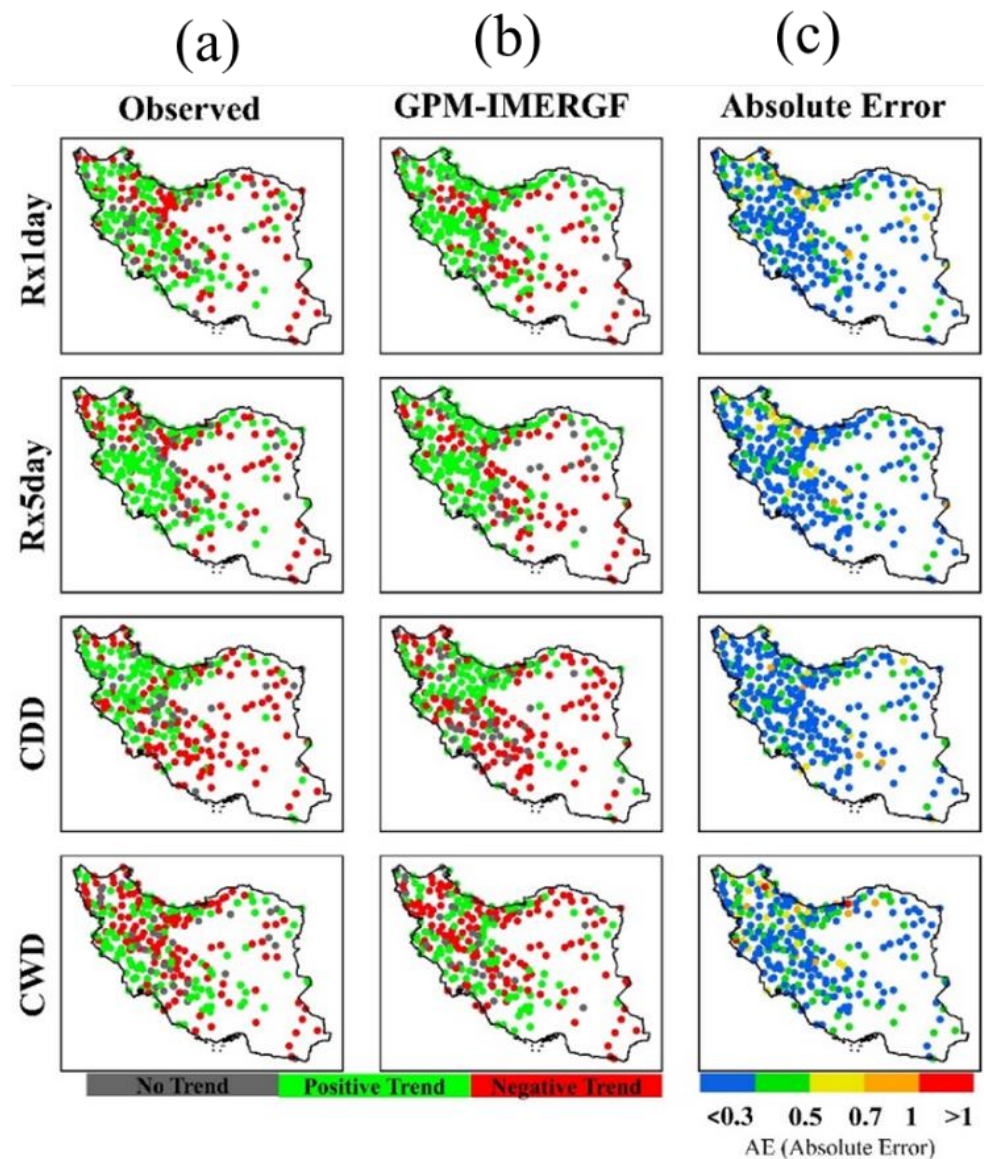
Figure 8. Maximum precipitation indices trends based on GPM-IMERGV6.0 Final Run (GPM-IMERGF) dataset and the observed data. (**a**–**c**) are observational trends, GPM-IMERGF estimated trends, and absolute error between estimated Tau Kendall (Z score) and observed ones, respectively.

Figure 9 shows the trend for R95pTOT and R99pTOT based on in situ and GPM-IMERGF datasets. The results showed a general agreement between the observed and estimated patterns of trends for R95pTOT and R99pTOT. Both datasets show a positive trend over the coast of Caspian, Alborz, and Zagros, while the other parts of the study area mainly present a negative trend, which is captured well by GPM-IMERGF (AE < 0.3). Like maximum precipitation indices, most negative trends were mainly found across arid regions (Extra-Arid, Arid, and Semi-Arid regions), while positive trends were mainly dominant across northern and western humid regions. The results also showed that the absolute error for GPM-IMERGF mainly was laid in the optimum range (AE < 0.3), however, there were some regions with higher absolute error (AE > 0.5) that is scattered unevenly across the study region.
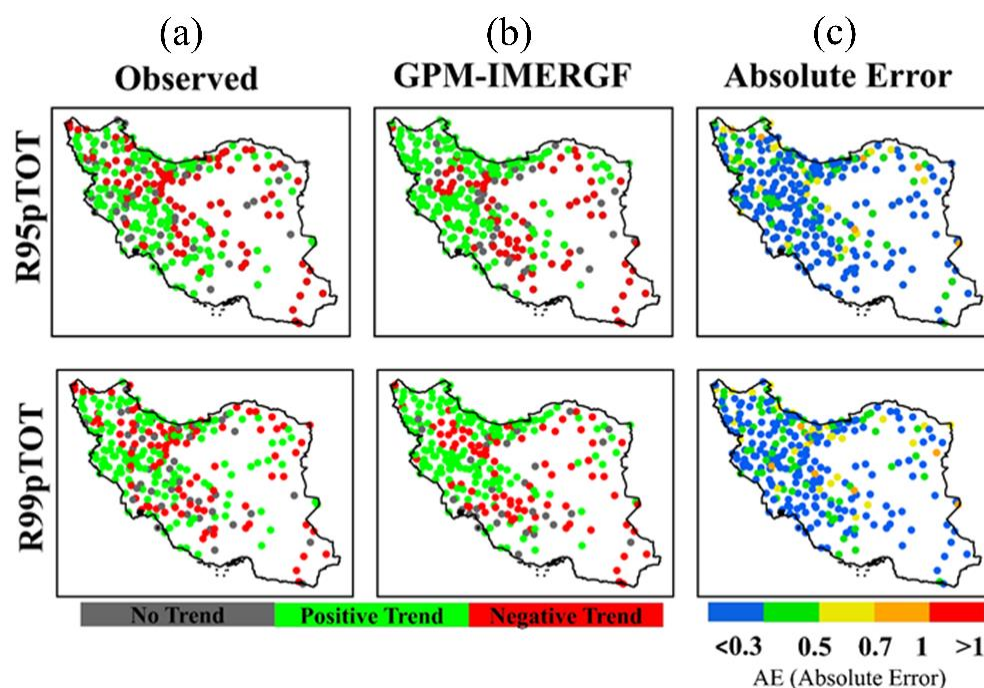
Figure 9. Percentile precipitation indices trends based on GPM-IMERGV6.0 Final Run (GPM-IMERGF) data and observational data. (**a**–**c**) are observational trends, GPM-IMERGF estimated trends, and absolute error between estimated Tau Kendall (Z score) and observed ones, respectively.

Based on Figure 10, there is a good agreement between the in situ observations and GPM-IMERGF regarding Absolute threshold indices. R10mm and R20mm depict a positive trend across Caspian, Alborz, and Zagros high altitude, which GPM-IMERGF reasonably captures (AE < 0.3). Regarding SDII and PRCPTOT indices, the results show that GPM-IMERGF has an excellent ability to capture trends all over the study area. Similar to maximum and percentile indices, the positive and negative trends were mainly scattered along humid and arid regions. However, compared to other groups, there were relatively negative trends in northern areas. Regarding the absolute error, it is evident that GPM-IMERGF showed high accuracy in most stations except for some regions mainly scattered across northwestern parts of the country (AE > 0.5). However, the trend results showed that the poor results obtained by GPM-IMERGF did not follow a specific pattern similar to previous trends for maximum and percentile indices. Overall, positive trends were mainly scattered along the Zagros mountains and Caspian with humid climates, while the negative trends for these indices were mainly found across arid regions. The dominant positive trends of maximum precipitation indices, percentile indices, and absolute threshold indices indicated that throughout 2007–2016 the frequency and amount of the heavy precipitation had increased drastically, mainly across Zagros highlands that are in line with previous results from [52]. However, the results from [83] were different as they found that most indices had decreasing trends across the major parts of Iran. The different results obtained from various studies might be due to the different periods and sources of precipitation used.
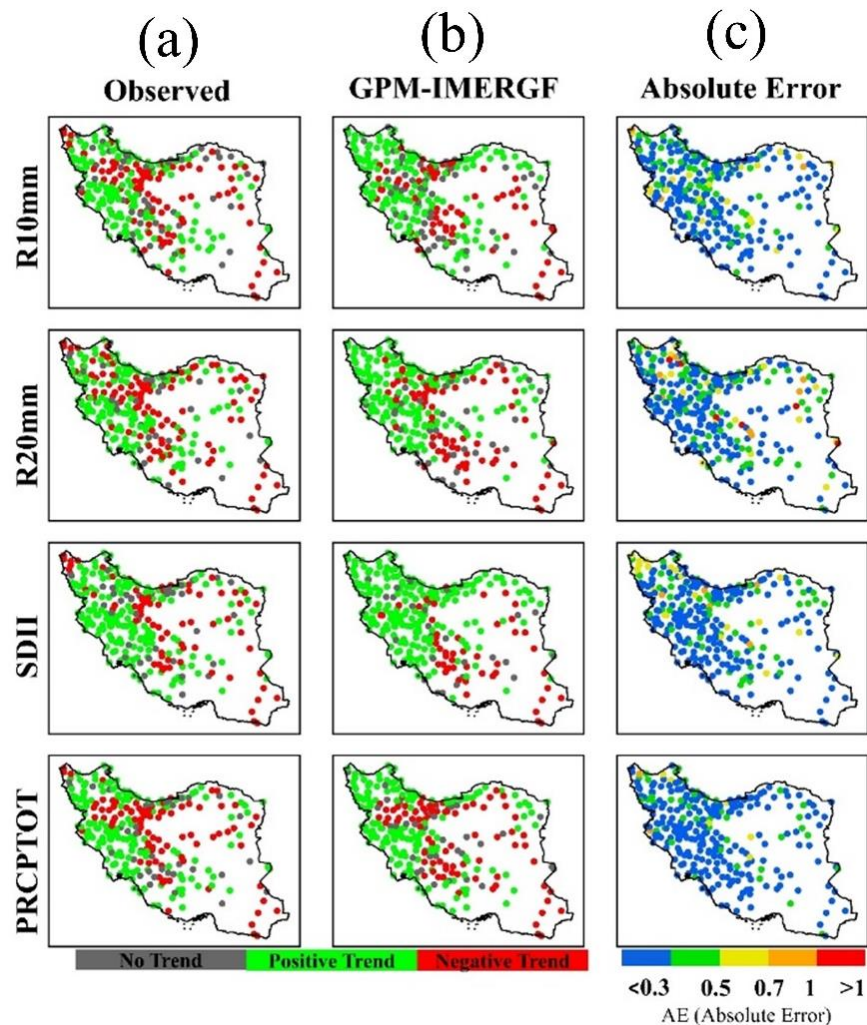
Figure 10. Absolute precipitation indices trends based on GPM-IMERGV6.0 Final Run (GPM-IMERGF) data and observational data. (**a**–**c**) are observational trends, GPM-IMERGF estimated trends, and absolute error between estimated Tau Kendall (Z score) and observed ones, respectively.

4. Summary and Conclusions

Figure 11 summarizes the overall performance of the GPM-IMERGF precipitation product among all indices in terms of median KGE scores. The results highlight a low to moderate accuracy in capturing maximum precipitation indices across different climate regions. Considering Rx1day and CWD indices, it is evident that GPM-IMERGF performs poorly for most climates (except for Humid and Arid climates in CWD), with KGE scores varying between 0 to 0.3. The results also indicate that the performance of GPM-IMERGF was slightly increased in capturing Rx5day indices with KGE > 0.4 for arid and semi-arid regions, as well as KGE > 0.3 for Humid, Semi-Humid, and Extra-Arid climates. GPM-IMERGF estimates CDD with similar accuracy to Rx5day (except for Semi-Arid regions), however, it fails to capture the CDD patterns over Semi-Humid climate with KGE < 0.1.

Considering GPM-IMERGF performance regarding percentile indices the KGE score varies between −0.34 to 0.28, indicating poor performance of the dataset in capturing the variability of R95pTOT and R99PTOT over different climate zones.
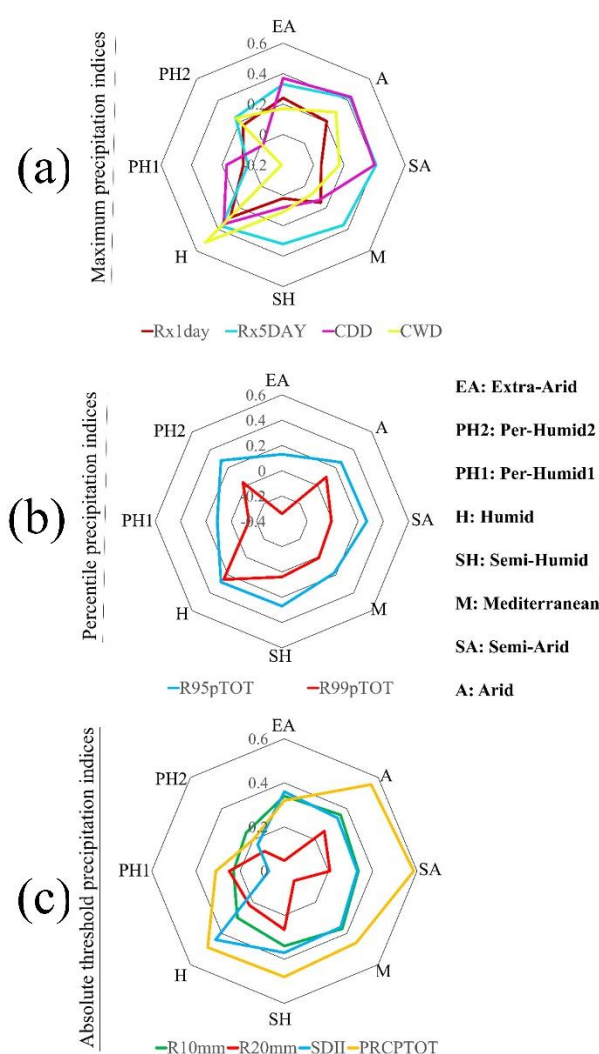
Figure 11. Summary of evaluations for all extreme precipitation indices over varying climate regions based on Kling-Gupta efficiency (KGE) index. (**a–c**) are representing maximum precipitation indices, percentile indices, and absolute threshold indices, respectively.

Based on the results from Figure 11, the overall performance of GPM-IMERGF in capturing R10mm and SDII indices is similar to each others (KGE varying between 0.3 to 0.4) for different climates (except for Per-Humid1 and Per-Humid2 classes). However, the results highlighted the poor performance of GPM-IMERGF in capturing the R20mm index with KGE < 0.26. The most robust performance by GPM-IMERGF is observed for the PRCPTOT with KGE within 0.3–0.6 for almost all climate regions (except for the Per-Humid2 class).

In this study, we have evaluated the GPM-IMERGF precipitation product in estimating extreme precipitation indices (maximum precipitation indices, percentile indices, and absolute threshold indices) over Iran, within 2007–2016. We have analyzed the performance of the datasets against a set of country-wide 281 synoptic stations using various statistical and visualization methods.

Based on the results of our analysis, the findings can be summarized as follows:

1. The results revealed that GPM-IMERGF had low to moderate accuracy regarding maximum precipitation indices based on different error metrics. However, relatively better performance of GPM-IMERGF was mainly found for Rx5day and CDD compared to other indices, especially over western parts of Iran.

2.   The best and the worst results for GPM-IMERGF were reported in capturing absolute threshold indices and percentile indices, respectively. GPM-IMERGF product was in good accordance with observational data in capturing PRCPTOT index across varying climate and topographies.

3.   The results also indicated that GPM-IMERGF was more effective in capturing R10mm index than R20mm higher accuracy across western Zagros mountainous regions.

4.   Considering extreme precipitation indices, statistical metrics indicated that GPM-IMERGF had low to moderate overestimation across arid regions. However, significant underestimation was observed over wet regions by GPM-IMERGF.

5.   Considering the spatial variation of different statistical metrics, it is evident that GPM-IMERGF estimations were more effective across Zagros mountainous regions. However, the worst results were obtained across northern coastal regions, dominated by a complex precipitation system.

6.   The trend analysis showed that GPM-IMERGF had acceptable accuracy regarding all precipitation indices based on the Mann–Kendall test. Furthermore, the results showed that most indices had mainly upward trend across the Zagros mountains and northern coastal regions.

The main contribution of this study is to assess the reliability of GPM-IMERGF in the context of extreme events while expanding our perception of the precipitation extremes variability over different climates of Iran. Floods and droughts may seem to be two independent events, but they are closely linked. Hence, studying extreme events in flood/drought-prone areas is essential for water resources planning and infrastructure design. GPM-IMERGF with high spatio-temporal resolution and proper latency covering extreme precipitation values with acceptable accuracy. However, applying statistical methods to provide rescaled data by eliminating the effects of over/underestimations such as bias correction is necessary, important shortcomings and drawbacks of GPM-IMERGF remains challenging and more deep error analysis needs to be considered from variety of aspects for this product. Moreover, it is evident from the results that GPM-IMERGF have major drawbacks across complex topographies. Another major issue in assessments of these products may attribute to gauge observations uncertainties which is worthy of attention for further researches. GPM-IMERGF data by feasible coverage of extreme values and anomalies could provide reliable data for hydrologic models, climate studies, and forecasting in the matter of extreme events, flood-drought propagation turns the GPM family into a long-standing member of global precipitation products.

Author Contributions: Author contributions were as follows: A.B., A.R., A.S. and J.T. equally contributed to data curation, methodology, visualization, result analysis and were mainly responsible for writing the paper; N.G. contributed to the writing, reviewing, and editing; P.S. lead the study, contributed to the methodology, result analysis, writing, reviewing, and editing. All authors have read and agreed to the published version of the manuscript.

Conflicts of Interest: The authors declare no conflict of interest.

Appendix A. Aridity Index

To examine the performance of GPM-IMERGF estimations regarding climate regions, we used Demartone Aridity Index [68] to identify climate zones for all stations. De Martonne classification system is a commonly used climate classification method based on Aridity Index (Equation (A1)). Based on aridity index stations mainly characterized by Semi-Arid regions (see Table A1)

$$AI = \frac{P}{T + 10} \tag{A1}$$

where P denotes Mean Annual Precipitation (MAP) in mm and T is mean annual temperature in Centigrade (°C).

Table A1. Climate zones of the studied stations based on De Martonne method.

Climate Regions	No. of Stations	Aridity Index
Extra-Arid	65	AI < 5
Arid	66	$5 \leq AI < 10$
Semi-Arid	110	$10 \leq AI < 20$
Mediterranean	9	$20 \leq AI < 24$
Semi-Humid	13	$24 \leq AI < 28$
Humid	5	$28 \leq AI < 35$
Per-Humid1	11	$35 \leq AI < 55$
Per-Humid2	2	≥ 55

References

1. Zhang, Q.; Sun, P.; Singh, V.P.; Chen, X. Spatial-temporal precipitation changes (1956–2000) and their implications for agriculture in China. *Glob. Planet. Chang.* **2012**, *82–83*, 86–95. [CrossRef]
2. Funk, C.C.; Peterson, P.J.; Landsfeld, M.F.; Pedreros, D.H.; Verdin, J.P.; Rowland, J.D.; Romero, B.E.; Husak, G.J.; Michaelsen, J.C.; Verdin, A.P. A Quasi-Global Precipitation Time Series for Drought Monitoring. In *U.S. Geological Survey Data Series*; Series 832; U.S. Geological Survey: Reston, VA, USA, 2014. [CrossRef]
3. Tapiador, F.J.; Kacimi, S.; De Castro, M.; Levizzani, V.; Katsanos, D.; García-Ortega, E. Precipitation Science: Observations, Retrievals, and Modeling. *Adv. Meteorol.* **2015**, *2015*, 843403. [CrossRef]
4. Pendergrass, A.G. What precipitation is extreme? *Science* **2018**, *360*, 1072–1073. [CrossRef] [PubMed]
5. Ghajarnia, N.; Kalantari, Z.; Destouni, G. Data-Driven Worldwide Quantification of Large-Scale Hydroclimatic Covariation Patterns and Comparison With Reanalysis and Earth System Modeling. *Water Resour. Res.* **2021**, *57*, e2020WR029377. [CrossRef]
6. Brida, A.B.; Owiyo, T.; Sokona, Y. Loss and damage from the double blow of flood and drought in Mozambique. *Int. J. Glob. Warm.* **2013**, *5*, 514–531. [CrossRef]
7. Devereux, S. The impact of droughts and floods on food security and policy options to alleviate negative effects. *Agric. Econ.* **2007**, *37*, 47–58. [CrossRef]
8. MESSNER, F.; MEYER, V. *Flood Damage, Vulnerability and Risk Perception – Challenges for Flood Damage Research. Flood Risk Manag. Hazards, Vulnerability Mitigation Measures*; Springer: Dordrecht, The Netherlands, 2006; pp. 149–167. [CrossRef]
9. Behboudian, M.; Kerachian, R. Evaluating the resilience of water resources management scenarios using the evidential reasoning approach: The Zarrinehrud river basin experience. *J. Environ. Manag.* **2021**, *284*, 112025. [CrossRef]
10. Myhre, G.; Alterskjær, K.; Stjern, C.W.; Hodnebrog; Marelle, L.; Samset, B.H.; Sillmann, J.; Schaller, N.; Fischer, E.; Schulz, M.; et al. Frequency of extreme precipitation increases extensively with event rareness under global warming. *Sci. Rep.* **2019**, *9*, 16063. [CrossRef]
11. Dehghani, M.; Salehi, S.; Mosavi, A.; Nabipour, N.; Shamshirband, S.; Ghamisi, P. Spatial analysis of seasonal precipitation over Iran: Co-variation with climate indices. *ISPRS Int. J. Geo Inf.* **2020**, *9*, 73. [CrossRef]
12. Ghaleni, M.M.; Sharafi, S.; Hosseini-Moghari, S.; Helali, J.; Oskouei, E.A. Spatiotemporal Characteristics of Meteorological Drought During the Past Half Century in Different Climates Over Iran. *Res. Sq.* **2022**. [CrossRef]
13. Tabari, H.; Nikbakht, J.; Hosseinzadeh Talaee, P. Hydrological Drought Assessment in Northwestern Iran Based on Streamflow Drought Index (SDI). *Water Resour. Manag.* **2013**, *27*, 137–151. [CrossRef]
14. Saemian, P.; Elmi, O.; Vishwakarma, B.D.; Tourian, M.J.; Sneeuw, N. Analyzing the Lake Urmia restoration progress using ground-based and spaceborne observations. *Sci. Total Environ.* **2020**, *739*, 139857. [CrossRef] [PubMed]
15. Voss, K.A.; Famiglietti, J.S.; Lo, M.; De Linage, C.; Rodell, M.; Swenson, S.C. Groundwater depletion in the Middle East from GRACE with implications for transboundary water management in the Tigris-Euphrates-Western Iran region. *Water Resour. Res.* **2013**, *49*, 904–914. [CrossRef]
16. Noori, R.; Maghrebi, M.; Mirchi, A.; Tang, Q.; Bhattarai, R.; Sadegh, M.; Noury, M.; Haghighi, A.T.; Kløve, B.; Madani, K. Anthropogenic depletion of Iran's aquifers. *Proc. Natl. Acad. Sci. USA* **2021**, *118*. [CrossRef]
17. Yadollahie, M. The flood in Iran: A consequence of the global warming? *Int. J. Occup. Environ. Med.* **2019**, *10*, 54–56. [CrossRef]

18.	Iran Floods Death Toll Reaches 70. Available online: https://www.france24.com/en/20190405-iran-floods-death-toll-reaches-70 (accessed on 5 April 2019).

19.	*Al Jazeera Iran Suffers "$2bn in Damages" as Flood Toll Continues to Rise*; Al Jazeera: Doha, Qatar, 2019.

20.	Dezfuli, A. Rare atmospheric river caused record floods across the middle east. *Bull. Am. Meteorol. Soc.* **2020**, *101*, E394–E400. [CrossRef]

21.	Tapiador, F.J.; Turk, F.J.; Petersen, W.; Hou, A.Y.; García-Ortega, E.; Machado, L.A.T.; Angelis, C.F.; Salio, P.; Kidd, C.; Huffman, G.J.; et al. Global precipitation measurement: Methods, datasets and applications. *Atmos. Res.* **2012**, *104–105*, 70–97. [CrossRef]

22.	Dyras, I.; Serafin-Rek, D. The application of GIS technology for precipitation mapping. *Meteorol. Appl.* **2005**, *12*, 69–75. [CrossRef]

23.	Alexakis, D.D.; Hadjimitsis, D.G.; Agapiou, A. Integrated use of remote sensing, GIS and precipitation data for the assessment of soil erosion rate in the catchment area of "Yialias" in Cyprus. *Atmos. Res.* **2013**, *131*, 108–124. [CrossRef]

24.	Eini, M.R.; Rahmati, A.; Piniewski, M. Hydrological application and accuracy evaluation of PERSIANN satellite-based precipitation estimates over a humid continental climate catchment. *J. Hydrol. Reg. Stud.* **2022**, *41*, 101109. [CrossRef]

25.	Eini, M.R.; Olyaei, M.A.; Kamyab, T.; Teymoori, J.; Brocca, L.; Piniewski, M. Evaluating three non-gauge-corrected satellite precipitation estimates by a regional gauge interpolated dataset over Iran. *J. Hydrol. Reg. Stud.* **2021**, *38*, 100942. [CrossRef]

26.	Shayeghi, A.; Azizian, A.; Brocca, L. Reliability of reanalysis and remotely sensed precipitation products for hydrological simulation over the Sefidrood River Basin, Iran. *Hydrol. Sci. J.* **2020**, *65*, 296–310. [CrossRef]

27.	Ghajarnia, N.; Liaghat, A.; Arasteh, P.D. Comparison and evaluation of high resolution precipitation estimation products in Urmia Basin-Iran. *Atmos. Res.* **2015**, *158*, 50–65. [CrossRef]

28.	Ghajarnia, N.; Daneshkar Arasteh, P.; Liaghat, M.; Araghinejad, S. Error Analysis on PERSIANN Precipitation Estimations: Case Study of Urmia Lake Basin, Iran. *J. Hydrol. Eng.* **2018**, *23*, 05018006. [CrossRef]

29.	Akbari, M.; Ghajarnia, N.; Ghajarnia, N.; Akbari, M.; Saemian, P.; Ehsani, M.R.; Azizian, A.; Kalantari, Z.; Behrangi, A.; Tourian, M.J.; et al. Evaluating the Evolution of ECMWF Precipitation Products Using Observational Data for Iran: From ERA40 to ERA5. 2018. Available online: https://www.researchgate.net/publication/355009348_Evaluating_the_Evolution_of_ECMWF_Precipitation_Products_Using_Observational_Data_for_Iran_From_ERA40_to_ERA5 (accessed on 30 April 2022).

30.	Rahmati, A.; Bakhtar, A.; Shayeghi, A.; Kalantari, Z.; Massah Bavani, A.; Ghajarnia, N. Spatio-temporal performance evaluation of 14 global precipitation estimation products across river basins in southwest Iran 2. *Earth Space Sci. Open Arch.* **2021**.

31.	Rajulapati, C.R.; Papalexiou, S.M.; Clark, M.P.; Razavi, S.; Tang, G.; Pomeroy, J.W. Assessment of extremes in global precipitation products: How reliable are they? *J. Hydrometeorol.* **2020**, *21*, 2855–2873. [CrossRef]

32.	Scofield, R.A.; Kuligowski, R.J. Status and outlook of operational satellite precipitation algorithms for extreme-precipitation events. *Weather Forecast.* **2003**, *18*, 1037–1051. [CrossRef]

33.	Liu, J.; Xia, J.; She, D.; Li, L.; Wang, Q.; Zou, L. Evaluation of six satellite-based precipitation products and their ability for capturing characteristics of extreme precipitation events over a climate transition area in China. *Remote Sens.* **2019**, *11*, 1477. [CrossRef]

34.	Huffman, G.J.; Bolvin, D.T.; Braithwaite, D.; Hsu, K.; Joyce, R.; Xie, P.; Yoo, S.-H. NASA global precipitation measurement (GPM) integrated multi-satellite retrievals for GPM (IMERG). *Algorithm Theor. Basis Doc. Version* **2015**, *4*, 26.

35.	Fang, J.; Yang, W.; Luan, Y.; Du, J.; Lin, A.; Zhao, L. Evaluation of the TRMM 3B42 and GPM IMERG products for extreme precipitation analysis over China. *Atmos. Res.* **2019**, *223*, 24–38. [CrossRef]

36.	Huang, Y.; Chen, S.; Cao, Q.; Hong, Y.; Wu, B.; Huang, M.; Qiao, L.; Zhang, Z.; Li, Z.; Li, W.; et al. Evaluation of version-7 TRMM multi-satellite precipitation analysis product during the Beijing extreme heavy rainfall event of 21 July 2012. *Water* **2014**, *6*, 32–44. [CrossRef]

37.	Li, Z.; Tang, G.; Hong, Z.; Chen, M.; Gao, S.; Kirstetter, P.; Gourley, J.J.; Wen, Y.; Yami, T.; Nabih, S. Two-decades of GPM IMERG early and final run products intercomparison: Similarity and difference in climatology, rates, and extremes. *J. Hydrol.* **2021**, *594*, 125975. [CrossRef]

38.	Derin, Y.; Anagnostou, E.; Berne, A.; Borga, M.; Boudevillain, B.; Buytaert, W.; Chang, C.-H.; Chen, H.; Delrieu, G.; Hsu, Y.C. Evaluation of GPM-era global satellite precipitation products over multiple complex terrain regions. *Remote Sens.* **2019**, *11*, 2936. [CrossRef]

39.	Gaona, M.F.R.; Overeem, A.; Leijnse, H.; Uijlenhoet, R. First-year evaluation of GPM rainfall over the Netherlands: IMERG day 1 final run (V03D). *J. Hydrometeorol.* **2016**, *17*, 2799–2814. [CrossRef]

40.	Jiang, S.; Ren, L.; Xu, C.-Y.; Yong, B.; Yuan, F.; Liu, Y.; Yang, X.; Zeng, X. Statistical and hydrological evaluation of the latest Integrated Multi-satellitE Retrievals for GPM (IMERG) over a midlatitude humid basin in South China. *Atmos. Res.* **2018**, *214*, 418–429. [CrossRef]

41.	Tang, S.; Li, R.; He, J.; Wang, H.; Fan, X.; Yao, S. Comparative evaluation of the GPM IMERG early, late, and final hourly precipitation products using the CMPA data over Sichuan Basin of China. *Water* **2020**, *12*, 554. [CrossRef]

42.	Kim, K.; Park, J.; Baik, J.; Choi, M. Evaluation of topographical and seasonal feature using GPM IMERG and TRMM 3B42 over Far-East Asia. *Atmos. Res.* **2017**, *187*, 95–105. [CrossRef]

43.	Asong, Z.E.; Razavi, S.; Wheater, H.S.; Wong, J.S. Evaluation of Integrated Multisatellite Retrievals for GPM (IMERG) over southern Canada against ground precipitation observations: A preliminary assessment. *J. Hydrometeorol.* **2017**, *18*, 1033–1050. [CrossRef]

44. Wu, Y.; Zhang, Z.; Huang, Y.; Jin, Q.; Chen, X.; Chang, J. Evaluation of the GPM IMERG v5 and TRMM 3B42 v7 precipitation products in the Yangtze River basin, China. *Water* **2019**, *11*, 1459. [CrossRef]

45. Tang, G.; Ma, Y.; Long, D.; Zhong, L.; Hong, Y. Evaluation of GPM Day-1 IMERG and TMPA Version-7 legacy products over Mainland China at multiple spatiotemporal scales. *J. Hydrol.* **2016**, *533*, 152–167. [CrossRef]

46. Yu, L.; Leng, G.; Python, A.; Peng, J. A comprehensive evaluation of latest GPM IMERG V06 early, late and final precipitation products across China. *Remote Sens.* **2021**, *13*, 1208. [CrossRef]

47. Foelsche, U.; Kirchengast, G.; Fuchsberger, J.; Tan, J.; Petersen, W.A. Evaluation of GPM IMERG Early, Late, and Final rainfall estimates using WegenerNet gauge data in southeastern Austria. *Hydrol. Earth Syst. Sci.* **2017**, *21*, 6559–6572.

48. Wang, C.; Tang, G.; Han, Z.; Guo, X.; Hong, Y. Global intercomparison and regional evaluation of GPM IMERG Version-03, Version-04 and its latest Version-05 precipitation products: Similarity, difference and improvements. *J. Hydrol.* **2018**, *564*, 342–356. [CrossRef]

49. Wang, Z.; Zhong, R.; Lai, C.; Chen, J. Evaluation of the GPM IMERG satellite-based precipitation products and the hydrological utility. *Atmos. Res.* **2017**, *196*, 151–163. [CrossRef]

50. Alavinia, S.H.; Zarei, M. Analysis of spatial changes of extreme precipitation and temperature in Iran over a 50-year period. *Int. J. Climatol.* **2021**, *41*, E2269–E2289. [CrossRef]

51. Asgari, A.; Rahimzadeh, F.; Mohammadian, N.; Fattahi, E. Trend Analysis of Extreme Precipitation Indices Over Iran. *Iran-Water Resour. Res.* **2007**, *3*, 42–55.

52. Balling, R.C.; Keikhosravi Kiany, M.S.; Sen Roy, S.; Khoshhal, J. Trends in Extreme Precipitation Indices in Iran: 1951-2007. *Adv. Meteorol.* **2016**, *2016*, 2456809. [CrossRef]

53. Darand, M.; Dostkamyan, M.; Rehmani, M.I.A. Spatial autocorrelation analysis of extreme precipitation in Iran. *Russ. Meteorol. Hydrol.* **2017**, *42*, 415–424. [CrossRef]

54. Esmaeilpour, M.; Ghasemi, A.R.; Khoramabadi, F.; Rashedi, S. Spatiotemporal variability of trend in extreme precipitations using fuzzy clustering over Northwest Iran. *Earth Sci. Inform.* **2021**, *14*, 2123–2132. [CrossRef]

55. Mohammadi, H.; Azizi, G.; Khoshahklagh, F.; Ranjbar, F. Analysis of daily precipitation extreme indices trend in Iran. *Phys. Geogr. Res. Q.* **2017**, *49*, 21–37.

56. Rahimi, M.; Mohammadian, N.; Vanashi, A.R.; Whan, K. Trends in indices of extreme temperature and precipitation in iran over the period 1960-2014. *Open J. Ecol.* **2018**, *8*, 396–415. [CrossRef]

57. Rahimi, M.; Fatemi, S.S. Mean versus extreme precipitation trends in Iran over the period 1960–2017. *Pure Appl. Geophys.* **2019**, *176*, 3717–3735. [CrossRef]

58. Rousta, I.; Soltani, M.; Zhou, W.; Cheung, H.H.N. Analysis of extreme precipitation events over central plateau of Iran. *Am. J. Clim. Chang.* **2016**, *5*, 297–313. [CrossRef]

59. Katiraie-Boroujerdy, P.S.; Akbari Asanjan, A.; Hsu, K.L.; Sorooshian, S. Intercomparison of PERSIANN-CDR and TRMM-3B42V7 precipitation estimates at monthly and daily time scales. *Atmos. Res.* **2017**, *193*, 36–49. [CrossRef]

60. Keikhosravi Kiany, M.S.; Masoodian, S.A.; Balling, R.C.; Montazeri, M.; Kiany, M.S.K.; Masoodian, S.A.; Balling, R.C., Jr.; Montazeri, M. Evaluation of the TRMM 3B42 product for extreme precipitation analysis over southwestern Iran. *Adv. Sp. Res.* **2020**, *66*, 2094–2112. [CrossRef]

61. Hosseini-Moghari, S.-M.; Tang, Q. Validation of GPM IMERG V05 and V06 Precipitation Products over Iran. *J. Hydrometeorol.* **2020**, *21*, 1011–1037. [CrossRef]

62. Saemian, P.; Hosseini-Moghari, S.M.; Fatehi, I.; Shoarinezhad, V.; Modiri, E.; Tourian, M.J.; Tang, Q.; Nowak, W.; Bárdossy, A.; Sneeuw, N. Comprehensive evaluation of precipitation datasets over Iran. *J. Hydrol.* **2021**, *603*. [CrossRef]

63. Sharifi, E.; Saghafian, B.; Steinacker, R. Downscaling Satellite Precipitation Estimates With Multiple Linear Regression, Artificial Neural Networks, and Spline Interpolation Techniques. *J. Geophys. Res. Atmos.* **2019**, *124*, 789–805. [CrossRef]

64. Khodadoust Siuki, S.; Saghafian, B.; Moazami, S. Comprehensive evaluation of 3-hourly TRMM and half-hourly GPM-IMERG satellite precipitation products. *Int. J. Remote Sens.* **2017**, *38*, 558–571. [CrossRef]

65. Moazami, S.; Golian, S.; Hong, Y.; Sheng, C.; Kavianpour, M.R. Comprehensive evaluation of four high-resolution satellite precipitation products under diverse climate conditions in Iran. *Hydrol. Sci. J.* **2016**, *61*, 420–440. [CrossRef]

66. Miri, M.; Masoudi, R.; Raziei, T. Performance Evaluation of Three Satellites-Based Precipitation Data Sets Over Iran. *J. Indian Soc. Remote Sens.* **2019**, *47*, 2073–2084. [CrossRef]

67. Sadeqi, A.; Kahya, E. Spatiotemporal analysis of air temperature indices, aridity conditions, and precipitation in Iran. *Theor. Appl. Climatol.* **2021**, *145*, 703–716. [CrossRef]

68. de Martonne, E. Une nouvelle function climatologique: L'indice d'aridité. *Meteorologie* **1926**, *2*, 449–459.

69. Rahimi, J.; Ebrahimpour, M.; Khalili, A. Spatial changes of extended De Martonne climatic zones affected by climate change in Iran. *Theor. Appl. Climatol.* **2013**, *112*, 409–418. [CrossRef]

70. Koohi, S.; Azizian, A.; Brocca, L. Spatiotemporal drought monitoring using bottom-up precipitation dataset (SM2RAIN-ASCAT) over different regions of Iran. *Sci. Total Environ.* **2021**, *779*, 146535. [CrossRef]

71. Darand, M.; Amanollahi, J.; Zandkarimi, S. Evaluation of the performance of TRMM Multi-satellite Precipitation Analysis (TMPA) estimation over Iran. *Atmos. Res.* **2017**, *190*, 121–127. [CrossRef]

72. Liu, C.; Zipser, E.J. The global distribution of largest, deepest, and most intense precipitation systems. *Geophys. Res. Lett.* **2015**, *42*, 3591–3595. [CrossRef]

73. Hou, A.Y.; Kakar, R.K.; Neeck, S.; Azarbarzin, A.A.; Kummerow, C.D.; Kojima, M.; Oki, R.; Nakamura, K.; Iguchi, T. The global precipitation measurement mission. *Bull. Am. Meteorol. Soc.* **2014**, *95*, 701–722. [CrossRef]

74. Smith, E.A.; Asrar, G.; Furuhama, Y.; Ginati, A.; Mugnai, A.; Nakamura, K.; Adler, R.F.; Chou, M.D.; Desbois, M.; Durning, J.F.; et al. International global precipitation measurement (GPM) program and mission: An overview. *Adv. Glob. Chang. Res.* **2007**, *28*, 611–653. [CrossRef]

75. From TRMM to GPM: The Evolution of NASA Precipitation Data | Earthdata. Available online: https://earthdata.nasa.gov/learn/articles/tools-and-technology-articles/trmm-to-gpm (accessed on 29 September 2015).

76. Draper, D.W.; Newell, D.A.; Wentz, F.J.; Krimchansky, S.; Skofronick-Jackson, G.M. The Global Precipitation Measurement (GPM) microwave imager (GMI): Instrument overview and early on-orbit performance. *IEEE J. Sel. Top. Appl. Earth Obs. Remote Sens.* **2015**, *8*, 3452–3462. [CrossRef]

77. Wang, J.; Houze, R.A.; Fan, J.; Brodzik, S.R.; Feng, Z.; Hardin, J.C. The detection of mesoscale convective systems by the GPM Ku-band spaceborne radar. *J. Meteorol. Soc. Jpn.* **2019**, *97*, 1059–1073. [CrossRef]

78. Huffman, G.J.; Bolvin, D.T.; Braithwaite, D.; Hsu, K.-L.; Joyce, R.J.; Kidd, C.; Nelkin, E.J.; Sorooshian, S.; Stocker, E.F.; Tan, J. Integrated multi-satellite retrievals for the Global Precipitation Measurement (GPM) mission (IMERG). In *Satellite Precipitation Measurement*; Springer: Cham, Switzerland, 2020; pp. 343–353.

79. Tan, J.; Huffman, G.J.; Bolvin, D.T.; Nelkin, E.J. IMERG V06: Changes to the morphing algorithm. *J. Atmos. Ocean. Technol.* **2019**, *36*, 2471–2482. [CrossRef]

80. Karki, R.; Hasson, S.U.; Schickhoff, U.; Scholten, T.; Böhner, J. Rising precipitation extremes across Nepal. *Climate* **2017**, *5*, 4. [CrossRef]

81. Casanueva, A.; Rodríguez-Puebla, C.; Frías, M.D.; González-Reviriego, N. Variability of extreme precipitation over Europe and its relationships with teleconnection patterns. *Hydrol. Earth Syst. Sci.* **2014**, *18*, 709–725. [CrossRef]

82. Miao, C.; Ashouri, H.; Hsu, K.-L.; Sorooshian, S.; Duan, Q. Evaluation of the PERSIANN-CDR daily rainfall estimates in capturing the behavior of extreme precipitation events over China. *J. Hydrometeorol.* **2015**, *16*, 1387–1396. [CrossRef]

83. Katiraie-Boroujerdy, P.-S.; Ashouri, H.; Hsu, K.; Sorooshian, S. Trends of precipitation extreme indices over a subtropical semi-arid area using PERSIANN-CDR. *Theor. Appl. Climatol.* **2017**, *130*, 249–260. [CrossRef]

84. Gupta, H.V.; Kling, H.; Yilmaz, K.K.; Martinez, G.F. Decomposition of the mean squared error and NSE performance criteria: Implications for improving hydrological modelling. *J. Hydrol.* **2009**, *377*, 80–91. [CrossRef]

85. Kling, H.; Fuchs, M.; Paulin, M. Runoff conditions in the upper Danube basin under an ensemble of climate change scenarios. *J. Hydrol.* **2012**, *424*, 264–277. [CrossRef]

86. Mann, H.B. Nonparametric tests against trend. *Econom. J. Econom. Soc.* **1945**, *13*, 245–259. [CrossRef]

87. Kendall, M.G. *Rank Correlation Methods*; American Psychological Association: Washington, DC, USA, 1948.

88. Amjad, M.; Yilmaz, M.T.; Yucel, I.; Yilmaz, K.K. Performance evaluation of satellite- and model-based precipitation products over varying climate and complex topography. *J. Hydrol.* **2020**, *584*, 124707. [CrossRef]

89. Fallah, A.; Rakhshandehroo, G.R.; Berg, P.; O, S.; Orth, R. Evaluation of precipitation datasets against local observations in southwestern Iran. *Int. J. Climatol.* **2020**, *40*, 4102–4116. [CrossRef]